Satellite Navigation
https://satellite-navigation.springeropen.com/

ORIGINAL ARTICLE

Open Access

Retrieval of sea ice thickness using FY-3E/GNOS-II data

Yunjian Xie[1] and Qingyun Yan[1*]

Abstract

Sea ice, a significant component in polar regions, plays a crucial role in climate change through its varying conditions. In Global Navigation Satellite System-Reflectometry (GNSS-R) studies, the observed surface reflectivity Γ serves as a tool to examine the physical characteristics of sea ice covers. This facilitates the large-scale estimation of first-year ice thickness using a two-layer sea ice-seawater medium model. However, it is important to note that when Sea Ice Thickness (SIT) becomes thicker, the accuracy of SIT retrieval via this two-layer model begins to decline. In this paper, we present a novel application of a spaceborne GNSS-R technique to retrieve SIT based on a three-layer model using the data from Fengyun-3E (FY-3E). Soil Moisture Ocean Salinity (SMOS) data are treated as the reference. The performance of the proposed three-layer model is evaluated against a previously established two-layer model for SIT retrieval. The analysis used the sea ice data from 2022 and 2023 with SITs less than 1.1 m. By comparing the retrieved SITs against reference values, the three-layer model achieved a Root Mean Square Error (RMSE) of 0.149 m and Correlation Coefficient (r) of 0.830, while the two-layer model reported the RMSE of 0.162 m and r value of 0.789. A scheme incorporating both models yielded superior results than either individual model, with the RMSE of 0.137 m and r reaching up to 0.852. This study is the first application of FY-3E for GNSS-R SIT retrieval, combining the advantages of a two-layer model and a three-layer model and extending the precision of GNSS-R retrieval for SIT to within 1.1 m. This provides a good reference for the future studies on GNSS-R SIT retrieval.

Keywords Global navigation satellite system-reflectometry, Sea ice thickness, Fengyun-3E GNSS occultation sounder II (FY-3E/GNOS-II), Soil moisture ocean salinity

Introduction

Sea ice, with its pivotal role in the polar circle, has attracted a considerable attention the scientific community due to mounting concerns about climate change (Hartmann et al., 2013). Furthermore, it holds significant practical implications for marine resource development, maritime transportation, and polar expeditions among others (Yan & Huang, 2019). Notably, a substantial reduction in Arctic sea ice has been observed recently, underlining the increasing importance in studying Sea Ice Thickness (SIT). SIT is a key indicator of climate change, and its precise determination can aid in accurate modeling and prediction of future climatic scenarios. Therefore, SIT has emerged to play a formidable role in our concern for better understanding of earth's polar regions under the critical lens of climate change. However, in situ measurements of SIT are cumbersome and have a limited spatial coverage. In contrast, remote sensing provides a more efficient and economical option for obtaining SIT data.

Currently, large-scale SIT records primarily originate from remote sensing satellites. SIT can be retrieved using passive microwave sensors, scatterometers, radar altimetry, and Synthetic Aperture Radar (SAR). Given that passive microwave sensor and scatterometer data exhibit low spatial resolution (typically 25–50 km), whereas SAR

*Correspondence:
Qingyun Yan
003257@nuist.edu.cn
[1] School of Remote Sensing and Geomatics Engineering, Nanjing University of Information Science and Technology, Nanjing 210044, China

and radar altimetry offer higher resolution, and the latter are more frequently employed for SIT estimation. This includes platforms such as CryoSat-2 (CS-2) (Tilling et al., 2016), European Remote Sensing satellite-1 (ERS-1), and ERS-2 (Laxon et al., 2003). Despite their capacity to deliver high-quality SIT products, these radar satellites face challenges due to high operational costs and low temporal resolution. Additionally, empirical re-tracking used for altimeters lacks a concrete physical model. The interpretation of SAR images is often subjective and time-consuming.

Global Navigation Satellite System-Reflectometry (GNSS-R) presents a promising solution to these issues. It is an emerging remote sensing technique that leverages the signals transmitted by Global Navigation Satellite System (GNSS) satellites, such as those from the Global Positioning System (GPS), Galileo satellite navigation system (Galileo), Global'naya Navigatsionnaya Sputnikovaya Sistema (GLONASS), and BeiDou Navigation Satellite System (BDS). These GNSS signals are reflected off Earth's surface features, and the reflected signals are collected and analyzed to infer geophysical parameters. It operates under all weather conditions, offering advantages such as low costs and extensive coverage. GNSS-R has found wide applications in the studies related to ocean surface roughness and wind monitoring (Garrison et al., 2002; Li & Huang, 2014; Li et al., 2023; Yan et al., 2017), snow depth estimation (Jin & Najibi, 2014; Jin et al., 2016; Larson et al., 2009), and soil moisture retrieval (Camps et al., 2016; Katzberg et al., 2006; Yan et al., 2020).

However, the retrieval of SIT using spaceborne GNSS-R needs further exploration. A two-layer model initially showcased its effectiveness and efficiency using TechDemoSat-1 (TDS-1) reflectivity Γ data (Yan & Huang, 2020). That study utilized two-year TDS-1 data with 18,511 samples. The two-layer model that considers the attenuation by sea ice and the reflection on the sea ice-water interface (R_2) but ignores the reflection on the upper air-ice boundary (R_1, as shown in Fig. 1) provided SIT estimates essentially for thin ice. As the SIT increases, the results retrieved with the two-layer model begins to saturate progressively and exhibits poor performance in fitting thick ice due to the neglect of R_1. Hence, there is a necessity to explore the complete form of the three-layer model for thick ices.

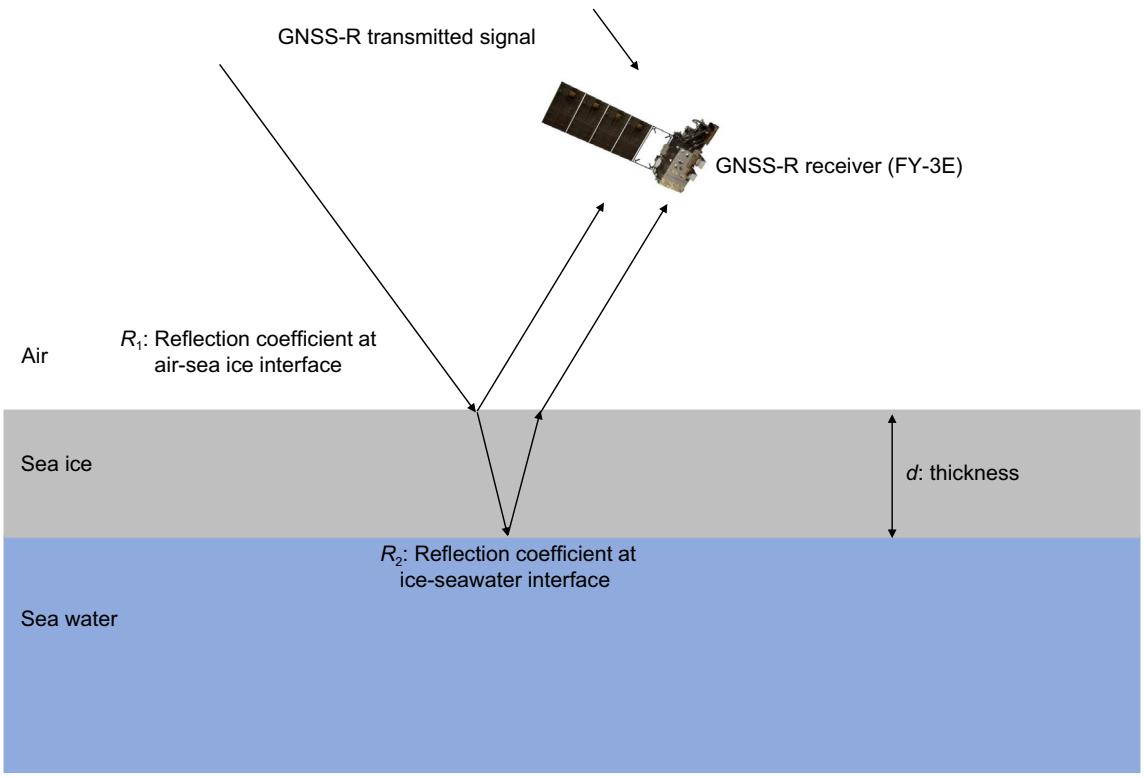

Fig. 1 Schematic of the three-layer model for the GNOS-R signal. For coherent reflections, the reflectivity (Γ) can be combined with the Fresnel reflection coefficient (R) and the SIT to construct a three-layer model. GNSS signals are sent from the transmitter and received either directly or after reflection through a three-layer model of air, sea ice, and seawater. R_1 and R_2 represent the reflection coefficients at the upper (air-sea ice) and lower (sea ice-seawater) interfaces, respectively, d is SIT. Therefore, in the three-layer model, the SIT can be estimated by the Γ of FY-3E

Meanwhile, with TDS-1 ceasing operations in May 2019, a gap in GNSS-R data in the polar regions emerged. This gap has since been filled by the Fengyun-3E GNSS Occultation Sounder-II (FY-3E/GNOS-II), which has provided GNSS-R data since March 2022. Notably, the application of FY-3E data in SIT retrieval has not been conducted thus far. In this paper, we first examine the three-layer model for SIT retrieval. Furthermore, we integrate the retrievals with both two- and three-layer models for different scenarios, enabling more precise estimates. This work signifies the first application of the three-layer model for SIT estimation using FY-3E data.

The remainder of this paper is structured in the following manner: Section "Dataset" provides a detailed description of the FY-3E GNOS-R data and Soil Moisture Ocean Salinity (SMOS) Level-3 (L3) SIT datasets, laying the foundation for subsequent discussions. Section "Modeling sea ice thickness retrieval" introduces the two-layer and three-layer models for estimating SIT, offering an in-depth exploration of their underlying methodologies. Subsequently, Section "Comparison and validation of retrieved SIT" presents our findings and engages in a comprehensive discussion about their implications, as well as a method that combines the respective strengths of the two models. Finally, we draw our conclusions in Section "Conclusion", summarizing key points and offering a comprehensive perspective of our study's outcomes.

Datasets

FY-3E GNOS-R

The FY-3E meteorological satellite, launched by China Meteorological Administration (CMA) on July 5, 2021, operates in a sun-synchronous orbit. It is positioned at an orbital altitude of 836 km and completes an orbital period in approximately 102 min. The daily observation scope of FY-3E encompasses the ocean surface, landmasses, and ice within latitudes ± 85°. With a revisit time of approximately every five-and-a-half days, GNOS-II provides nearly global coverage, presenting a notable advantage for comprehensive data collection. To cater for diverse applications like data assimilation and atmospheric/ionospheric inversion, GNOS-II data preprocessing currently produces three primary products: atmospheric additional phase, ionospheric additional phase, and GNSS reflection. The launched FY-3F/3G/3H satellites also incorporate GNOS-II sensors, contributing to the establishment of an extensive GNOS-R network.

Figure 2 provides visual representation of this extensive reach which illustrates the specular reflection points captured by the FY-3E GNOS-R over one day (on November 1st, 2022). This figure demonstrates that the satellite can efficiently receive reflected signals of GNSS satellites on a nearly global scale in a relatively short period.

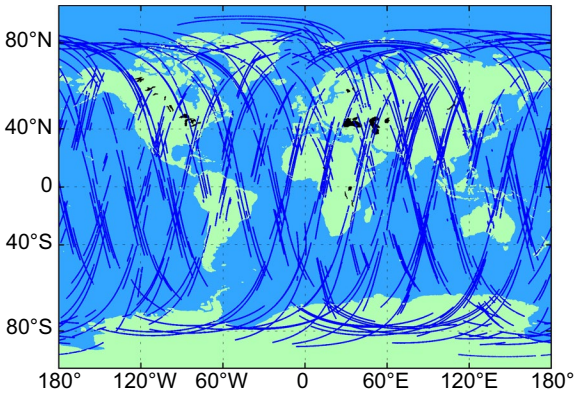

Fig. 2 Specular reflection points of FY-3E on November 1, 2022. GNOS-R can detect the complex and variable surface of the globe over a latitude range of ± 85° with an average revisit time of about 5.5 days. As a result, it can provide data with almost global coverage. The location of the surface reflection points received by the FY-3E GNOS-II on a single day are marked with blue dots in the latitude/longitude grid

The GNOS-R system excels in its ability to receive the signals from both GPS and BDS, a notable improvement compared to the previous TDS-1 system, which exclusively handled GPS signals. This design allows users to harness the data from these two major global satellite navigation networks, providing a comprehensive service and expanding the available data sources by leveraging the strengths of both systems.

In GNSS-R, the important remote sensing parameter information, in addition to the widely used Delay-Doppler Mapping (DDM) and sea surface normalized scattering coefficient, Γ is also one of the important parameters. It can reflect many physical properties of reflective surfaces, such as roughness, dielectric constant, etc., and is a key parameter in our current study. According to the GNSS-R bistatic radar equation (Zavorotny et al., 2014), we can obtain the surface Γ from FY-3E:

$$\Gamma(\theta) = \frac{(R_r + R_t)^2 (P_{\mathrm{DDM}} - N)}{4\pi F R_t^2 R_r^2} \tag{1}$$

where R_r and R_t are the distances from the specular reflection points to the receiver and the transmitter, respectively, P_{DDM} is the peak DDM power, N refers to noise, and F is the Bistatic Radar Cross Section Factor (DDM BRCS-Factor), which can be readily obtained from FY-3E dataset.

The dataset employed in this study comprises the GNOS-R data collected from October 15, 2022 to April 15, 2023. This time frame aligns with the period of the

L3 SIT product provided by SMOS. This consistency ensures a reliable comparison and integration of data between these two sources for our analysis.

SMOS

The SMOS satellite has been delivering L3 SIT products to the public since 2010. This is achieved with a Microwave Imaging Radiometer using Aperture Synthesis (MIRAS). MIRAS measures L-band brightness temperatures at varying angles of incidence and polarizations, which are crucial parameters in remote sensing applications. These measurements enable SMOS to retrieve information about SIT in the Arctic region. The retrieval process relies on the data related to sea ice temperatures and salinity (Tian-Kunze et al., 2014). These two factors play a significant role as they directly influence the interaction between electromagnetic waves and sea ice, thereby affecting its observed brightness temperature.

The SMOS L3 provides comprehensive details about northern hemisphere's SIT for the latitudes above 50° from October through April each year starting from 2010. In addition to this primary dataset, it also includes supplementary information such as temperature values specific to individual sections of the oceanic surface covered by sea ice along with their respective salinities. Furthermore, it contains an uncertainty estimate associated with each recorded value for SIT. Data projection within these SMOS L3 products follows National Snow and Ice Data Center (NSIDC) polar stereographic grid system. Each cell or unit area within this grid corresponds spatially to the squares of about 12.5 km × 12.5 km on ground level, providing high coverage across ice-covered regions. An illustrative example can be seen in Fig. 3. Where we present an Arctic SIT map derived from SMOS observations dated October 25, 2022.

As reported by Tian-Kunze and Kaleschke (2021), a notable issue arises with the saturation of brightness temperature as SIT increases. This saturation effect can lead to an underestimation of the thickness for larger ice formations, which lowers the accuracy of the derived SIT values. To mitigate this problem and enhance the reliability of our analysis, we adopt a conservative approach towards data handling. Specifically, we consider the uncertainty values associated with each SIT measurement provided in the SMOS L3 product. The data points whose this uncertainty exceeds 1 m are discarded, as recommended in the manual's guidelines. In spite of its uncertainty, it is known from several validation experiments with SMOS SIT products that SMOS SIT products can better respond to the actual conditions of thin ice than other mainstream SIT products (e.g., CS-2) (Kaleschke et al., 2016), and better monitor the SIT in the pan-Arctic area (> 50° N) (Tietsche et al., 2018).

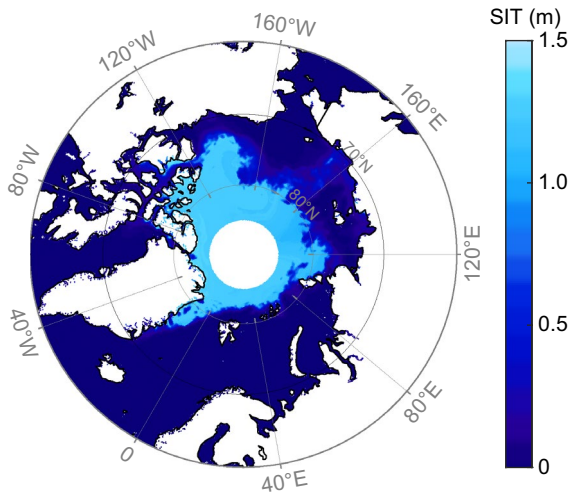

Fig. 3 SMOS SIT data on 25th October 2022. No data in the region is white

Modeling sea ice thickness retrieval

In terms of coherent reflection, Γ can be formulated as per (Tsang & Newton, 1982)

$$\Gamma = |R|^2 \cdot \exp\left[-\left(\tfrac{4\pi}{\lambda}\sigma_{\mathrm{RMS}}\sin\theta\right)^2\right] \tag{2}$$

Here σ_{RMS} represents the root mean square difference in height, and the exponential term in the equation accounts for roughness effects. Given that the σ_{RMS} of sea ice surface typically measures at centimeter level, it can be considered smooth within the GNSS-R domain (Yan & Huang, 2020). Consequently, the value of roughness term in this equation is approximately 1. Therefore, the Γ can be further approximated as

$$\Gamma = |R|^2 \tag{3}$$

R is the Fresnel reflection coefficient, which can be expressed as

$$R = \frac{R_1 + R_2 \mathrm{e}^{2ikd}}{1 + R_1 R_2 \mathrm{e}^{2ikd}} \tag{4}$$

$$k = \beta - j\alpha \tag{5}$$

$$\beta = \frac{2\pi}{\lambda}\cos\theta \mathrm{Re}\sqrt{\varepsilon_i} \tag{6}$$

$$\alpha = \frac{2\pi}{\lambda}\cos\theta \left|\mathrm{Im}\sqrt{\varepsilon_i}\right| \tag{7}$$

where d represents the SIT (as shown in Fig. 1), while k is the vertical component of the signal propagation vector,

determined by known signal wavelength λ, θ is satellite incidence angle, and ε_i is sea ice dielectric constant. Reflection coefficients at the upper (air-sea ice) and lower (sea ice-seawater) interfaces are denoted by R_1 and R_2, respectively, and their detailed formulas can be found in Yan and Huang (2020). α is the attenuation coefficient, and β is the phase constant.

The sea ice dielectric constant ε_i can be obtained from the Vant model (Vant et al., 1978), i.e.

$$\varepsilon_i = 3.1 + 0.0084 V_b + j(a_1 + a_2 V_b) \tag{8}$$

where V_b is the volume of brine and the coefficients a_1 and a_2 are 0.037 and 0.00445 in the case of first-year ice and 0.003 and 0.00435 in the case of multi-year ice, respectively. V_b can then be obtained from the Ulaby model (Ulaby et al., 1986),

$$V_b = 10^3 S\left(-\frac{49.185}{T} + 0.532\right) \tag{9}$$

where S and T are the salinity and temperature of sea ice. In addition, R_1 and R_2 are determined by the dielectric constant of each layer, which can be found by the following general formula,

$$R_{1,2} = \frac{1}{2}(R_{\mathrm{vv}} - R_{\mathrm{hh}}) \tag{10}$$

where R_{vv} and R_{hh} are the vertical polarization and horizontal polarization components, respectively, expressed by

$$R_{\mathrm{vv}} = \frac{\varepsilon_{1,2}\cos\theta_i - \sqrt{\varepsilon_{1,2} - \sin^2\theta_i}}{\varepsilon_{1,2}\cos\theta_i + \sqrt{\varepsilon_{1,2} - \sin^2\theta_i}} \tag{11}$$

$$R_{\mathrm{hh}} = \frac{\cos\theta_i - \sqrt{\varepsilon_{1,2} - \sin^2\theta_i}}{\cos\theta_i + \sqrt{\varepsilon_{1,2} - \sin^2\theta_i}} \tag{12}$$

$$\varepsilon_1 = \frac{\varepsilon_i}{1} \tag{13}$$

$$\varepsilon_1 = \frac{\varepsilon_w}{\varepsilon_i} \tag{14}$$

$$\theta_i = \arcsin\frac{\sin\theta}{\sqrt{\varepsilon_i}} \tag{15}$$

where ε_w is the dielectric constant of seawater, which can be obtained from the Klein-Swift model (Klein & Swift, 1977).

Combining the above expressions for the overall reflection coefficient of the three-layer of the medium, we can obtain

$$\Gamma = \left|\frac{R_1 + R_2 e^{-2ikd}}{1 + R_1 R_2 e^{-2ikd}}\right|^2 \tag{16}$$

Therefore, by combining the reflectivity with the overall reflectance coefficient, the expression for the relationship between reflectivity and SIT can be obtained, and the expression can be further derived and rewritten as

$$\Gamma = \frac{R_1^2 + 2R_1R_2\mathrm{e}^{-2\alpha d}\cos(2\beta d) + R_2^2\mathrm{e}^{-4\alpha d}}{1 + 2R_1R_2\mathrm{e}^{-2\alpha d}\cos(2\beta d) + R_1^2R_2^2\mathrm{e}^{-4\alpha d}} \tag{17}$$

At this point, a complete three-layer medium model of the signal traveling through the air to the sea ice and reflecting back to the receiver through the upper and lower interfaces of the sea ice has been established. The d can be calculated by solving for the reflectivity of the corresponding satellite reflection signal, combined with the altitude angle or incidence angle. It is worth noting that Yan and Huang (2020) disregarding the contribution of the upper interface may introduce errors when dealing with thick sea ice. This issue is addressed in this study by incorporating contributions from both layers. When R_1 is small, ignoring R_1 gives a two-layer model.

We found that the results of the three-layer model are worse than the two-layer model for thin ice in most cases. To address this, we propose a method to combine the results from both models, which can be found in Section "Comparison and validation of retrieved SIT". The flowchart of the FY-3E GNOS-R data retrieval SIT is shown in Fig. 4.

Comparison and validation of retrieved SIT

To ensure the integrity of our results and minimize the impact of potential errors, we implemented a comprehensive quality control strategy for our dataset. This strategy comprises four key steps:

1. We first limit our analysis to the data points where the incidence angle is less than 30° (Yan & Huang, 2020).
2. Secondly, we focus on the specular points where the Signal-to-Noise Ratio (SNR) exceeds 3 dB. By prioritizing high-SNR data points, we effectively reduce the interference of noise and enhance signal clarity.
3. Thirdly, we remove SMOS L3 SIT data with a SIT of 0 to eliminate the effect of seawater being mistaken as sea ice (Xie & Yan, 2024).
4. Lastly, for the SMOS L3 SIT dataset, we select only those the data points with associated uncertainties less than 1 m to ensure high confidence in each measurement used in our study.

After implementing a rigorous screening process and performing necessary data matching, a high-quality

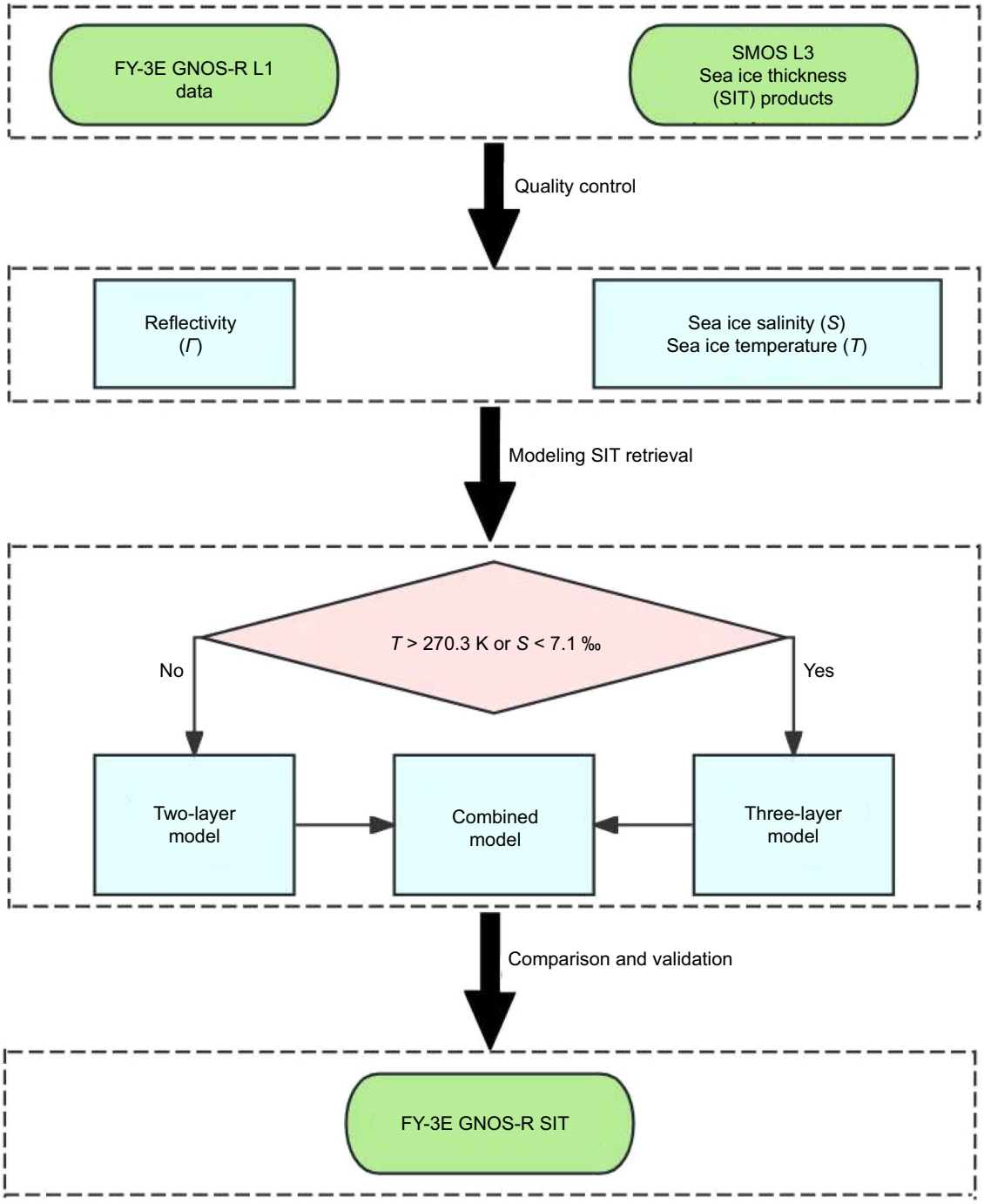

Fig. 4 The FY-3E GNOS-R data retrieval SIT flowchart. FY-3E data and SMOS L3 SIT data were quality controlled to obtain the Γ and S and T, respectively, and then the combined model was used in separate cases according to the thresholds set in S and T. The FY-3E GNOS-R retrieval of SIT was finally completed

dataset was obtained, comprising 36,534 samples. Specifically, there were 16,998 samples for GPS data and 19,536 samples for BDS data. This highlights BDS as a valuable resource for the SIT retrieval process.

Two-layer medium model

The two-layer model only considers the reflections on the sea ice-seawater interface (i.e., R_2) and ignores the reflections on the upper air-sea ice interface (setting R_1 to 0). While this simplifies the computation, it may not

be suitable for thicker or more signal-attenuating sea ice conditions.

Table 1 shows the results of the SIT retrieval and the estimated SIT using the full data with two-layer mode. Overall, the SIT obtained has an Root Mean Square Error (RMSE) of 0.162 m and a r of 0.789 compared to the SMOS SIT. Figure 5a shows the scatter density plot of the two-layer model SIT with reference SIT.

The FY-3E two-layer model SIT neglects the signal reflection R_1. This simplified model exhibits a satisfactory fit when the SMOS SIT is 0.5 m or less. However, as the SMOS SIT increases, the performance of the two-layer model degrades, suggesting less effective in estimating thicker SIT.

As Arctic temperatures decrease with the onset of the season, and sea ice begins to get thicken, the two-layer model demonstrates better performance, particularly during the initial stages when dealing with thinner first-year ice. However, its efficacy is reduced as SIT increases.

In addition, during the transitional period of March and April, a significant shift occurs in the state of sea ice due to the increase in temperatures. As the ice starts to melt, small puddles begin to form on its surface. These water bodies complicate the remote sensing process. In typical scenarios, the signals transmitted by satellite-based sensors are expected to interact primarily with the sea ice-seawater interface. However, with these surface puddles during melting periods, part of the signal can be reflected towards the receiver before it reaches this interface. This premature reflection can distort the measurements and result in errors in retrieving SIT. The phenomenon occurs because water bodies on the surface create an additional reflective interface that differs significantly from both sea ice and seawater in terms of dielectric properties. The reflections from these pools interfere with those originating from deeper layers, thus complicating interpretation and potentially leading to underestimation or overestimation errors. The presence of small puddles in the Arctic Sea ice described above is also seen and mentioned in Xie et al. (2020).

Three-layer medium model

The three-layer model offers a better simulation of the signal as it transmits through sea ice and returns to the receiver, making it more comprehensive and interpretable. The model addresses the scenario of simultaneous reflection of the signal in R_1 and R_2, making the resulting Eq. 17 complex and challenging to extract the formula for SIT (d). Thus, by following the relationship between d and Γ as depicted in Eq. 17, we performed a least-squares fitting to obtain d by substituting d produced in increments of 0.001 into Eq. 17. The option that aligns the closest is selected as the SIT determined by the three-layer model.

Table 1 presents the monthly outcomes of SIT retrievals and overall estimations with the three-layer model. Compared with SMOS SIT, the derived SIT demonstrated an RMSE value of 0.149 m and an r of 0.830. Figure 5b is the scatter density plot of the SIT against the reference SIT.

The three-layer model commonly adopted demonstrated suboptimal performance when dealing with partially thin ice. This limitation can be attributed to a phenomenon known as negative freeboard occurring within the sea ice (Li et al., 2021). Negative freeboard refers to a state where the sea level rises above the surface of the sea ice. In such cases, seawater covers portions of the sea ice, disrupting the traditional air-sea ice-seawater structure that underlies the three-layer model. When seawater overlays parts of the sea ice due to negative freeboard, it becomes part of the signal interaction process alongside air and sea ice layers. This additional interface causes the alteration in received signals since the reflections from seawater differ substantially from those originating from other layers. As a result, the measurements derived using this three-layer model can bias

Table 1 Retrieval accuracy of FY-3E SIT

Data	Results of two-layer model		Results of three-layer model		Results of combined model	
	RMSE (m)	r	RMSE (m)	r	RMSE (m)	r
2022–2010	0.094	0.856	0.094	0.867	0.079	0.903
2022–2011	0.135	0.851	0.132	0.873	0.117	0.898
2022–2012	0.157	0.830	0.139	0.863	0.123	0.892
2023–2001	0.147	0.807	0.149	0.833	0.133	0.863
2023–2002	0.164	0.774	0.161	0.812	0.146	0.838
2023–2003	0.204	0.740	0.177	0.781	0.168	0.811
2023–2004	0.213	0.718	0.175	0.773	0.167	0.813
All	0.162	0.789	0.149	0.830	0.137	0.852

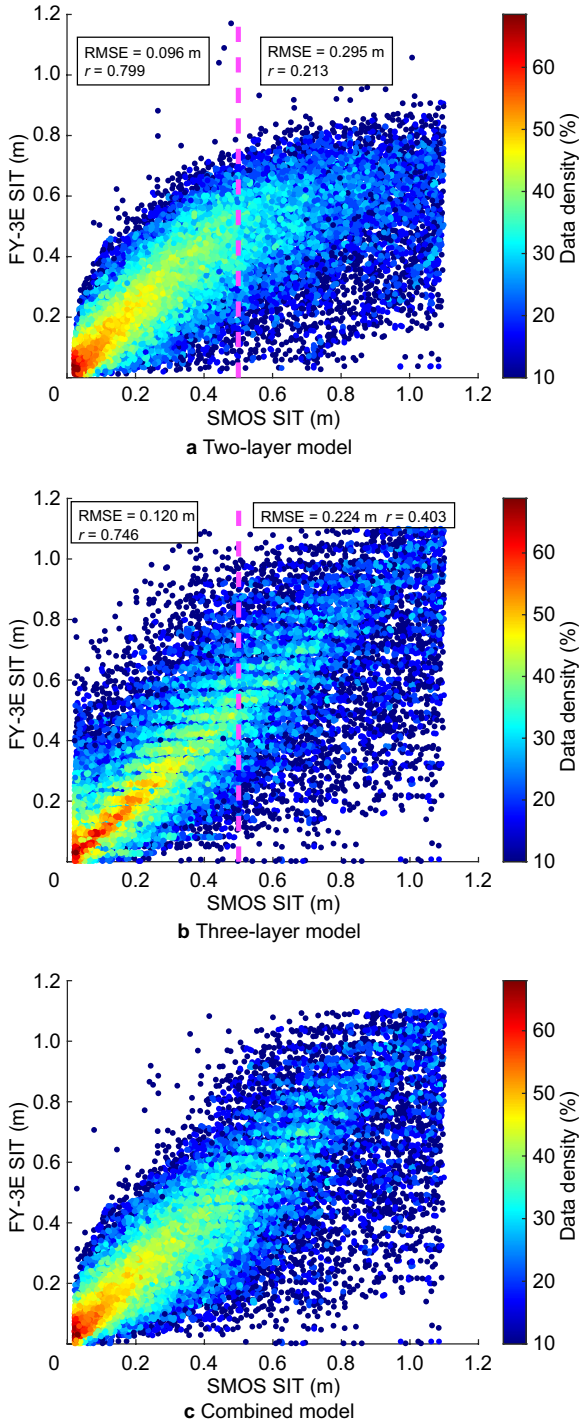

Fig. 5 Compare the SIT obtained by FY-3E with the reference SMOS data. Comparing (**a**) and (**b**), the RMSE and correlation coefficient (*r*) of the two-layer model are 0.096 m and 0.799 for SMOS SIT less than 0.5 m thin ice, which are better than those of the three-layer model (0.120 m and 0.746), while the opposite is for thick ice. (**c**) is a comparison of SIT with SMOS SIT estimated after combining the two-layer and three-layer models by *S* and *T*. The results are better than using one model alone

the estimates of SIT in the scenarios involving negative freeboard.

Combined model

In the data screening process, it was observed that the two-layer model offers a better fit than the three-layer model when handling thin reference SIT. Conversely, for thick reference SITs, the three-layer model is more suitable. Consequently, a suggestion is made to integrate both models as a combined model for more accurate SIT retrieval. Specific examples of this integration are depicted in Fig. 5a.

We extracted 1000 sets of SIT results with the two- and three-layer models in October 2022 as reference data and constructed various combination scenarios to enhance fitting and obtain more accurate SIT estimates. As illustrated in Fig. 7, a nonlinear relationship exists between SIT and its S and T. Generally, a higher T is associated with a smaller SIT, and a higher S corresponds to a smaller SIT.

Based on Fig. 6a, a comparison between the SIT results retrieved with the two- and the three-layer models reveals that the three-layer model in the upper box exhibits a better performance when the SIT exceeds approximately 0.5 m. In contrast, in the lower box, it is evident that while the two-layer model performs well in the presence of thin ice for the most part, there are the instances where its performance is not as robust as the three-layer model. With this observation and an analysis of Fig. 7 along with 1000 data sets and several experiments, we determined the final thresholds for S and T in the combined model, which are 7.1 ‰ and 270.3 K, respectively. Figure 8 visually illustrates the selection process employed during SIT retrieval with the combined model. This resulted in the formulation of a subsequent combination scheme:

$$\begin{cases} d = d_{\text{three}}, & T > 270.3\text{K}, \\ d = d_{\text{three}}, & S < 7.1\ ‰ \\ d = d_{\text{two}}, & T < 270.3\,\text{K or S} > 7.1\ ‰ \end{cases} \tag{18}$$

Applied to the data from the complete experimental period (October 2022 to April 2023), this combined method yielded an improved accuracy with an RMSE value of 0.137 m and an r of 0.852, surpassing the performance of either model used individually. The scatter density plots illustrating the relationship between retrieved SIT with this combined model and SMOS SIT are depicted in Fig. 5c. Detailed statistics for each month are in Table 1. We also present the SIT results by sample

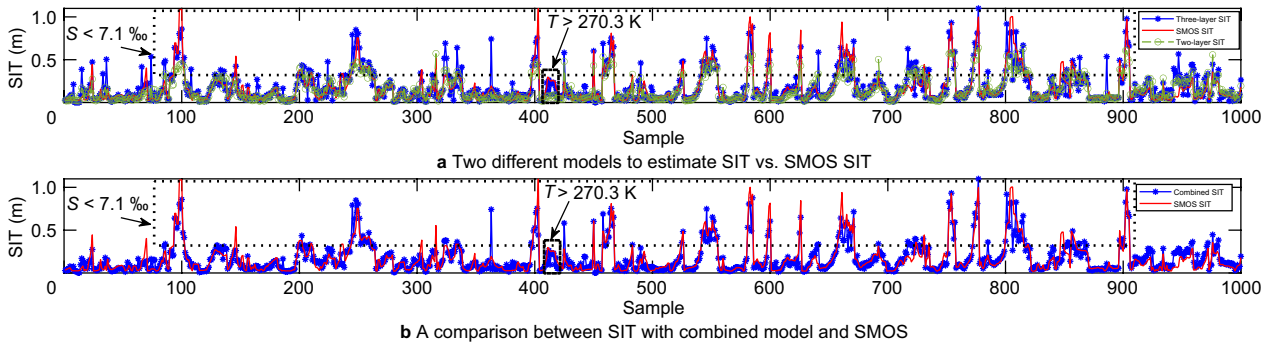

Fig. 6 The effects of the combined model versus the two-layer and three-layer models. In **a**, green is the SIT of the two-layer model, blue is the SIT of the three-layer model, and red is the SMOS SIT. The three-layer model has a better performance in the 1000 samples taken out when *S* is around 7.1 ‰, when the SMOS SIT is thick ice. The two-layer model performs better when *T* is around 270.3 K for thin ice. Combining the above, the effect of **b** is obtained after combining the two models, which improves the SIT retrieval accuracy

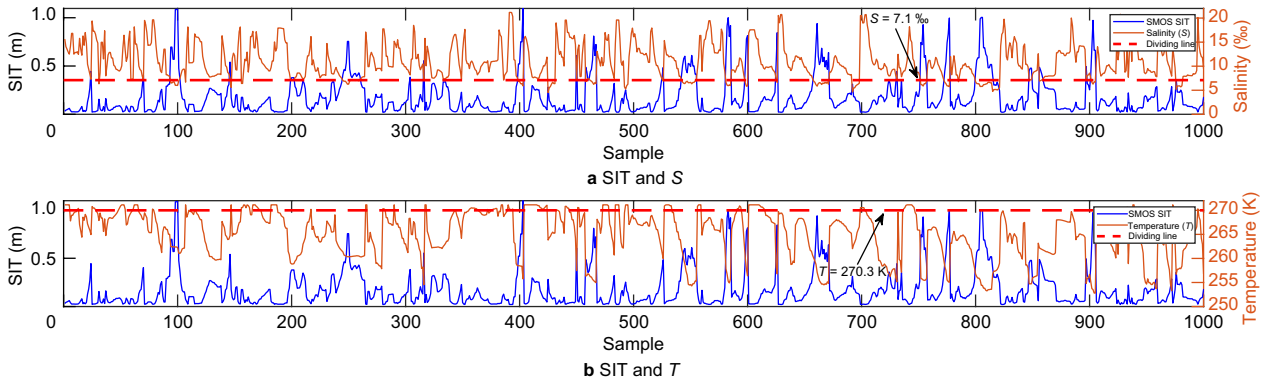

Fig. 7 Analyzing the SIT of SMOS in relation to *S* and *T* respectively. In **a**, *S* has a clear tendency to increase when SIT is thin ice, whereas in **b**, SIT is usually smaller for larger values of *T*. SIT has a certain nonlinear relationship with both *S* and *T*. A threshold is then specified to delineate between the use scenarios of the two-layer model and the three-layer model

(see Fig. 9 for October and November 2022) and display their spatial distribution (see Fig. 10 for the period from December 2022 to April 2023) for demonstration.

Error analysis

First, the presence of snow cover on sea ice surfaces can indeed complicate in the process of SIT estimation using GNSS-R. Snow, possessing different physical properties compared to sea ice, interacts differently with GNSS signals, altering the reflected signal's characteristics (Fung et al., 1994). Specifically, snow cover scatters and absorbs microwave signals differently, leading to the changes in amplitude, phase, or polarization state. Consequently, these alterations impact the interpretation and analysis of GNSS-R data in SIT estimation. Moreover, varying snow thickness affects signal attenuation or scattering, which needs to consider in GNSS-R data processing.

Second, the construction of two- and three-layer models for SIT estimation using GNSS-R data often needs an integration of empirical models and non-GNSS-R information. For instance, parameters such as *S* and *T* might need to be sourced from products like SMOS. However, this approach introduces potential error that can impact the accuracy of the retrieved SIT. Empirical models, by their very nature, are approximate that are based on observed data. While they can capture general trends or behaviors well, they may not fully account for all complex interactions or variability in real-world conditions. Consequently, any errors in these empirical models will propagate into the SIT estimates derived from them. Furthermore, the differences in spatial resolution between GNSS-R data and other datasets can lead to data mismatching when integrating different sources of data.

Third, the simultaneous reception of the reflected signals from different GNSS such as GPS, BDS, and Galileo also complicate SIT retrieval. This arises from potential differences in system-specific signal characteristics affecting reflectivity measurements. According to Yin

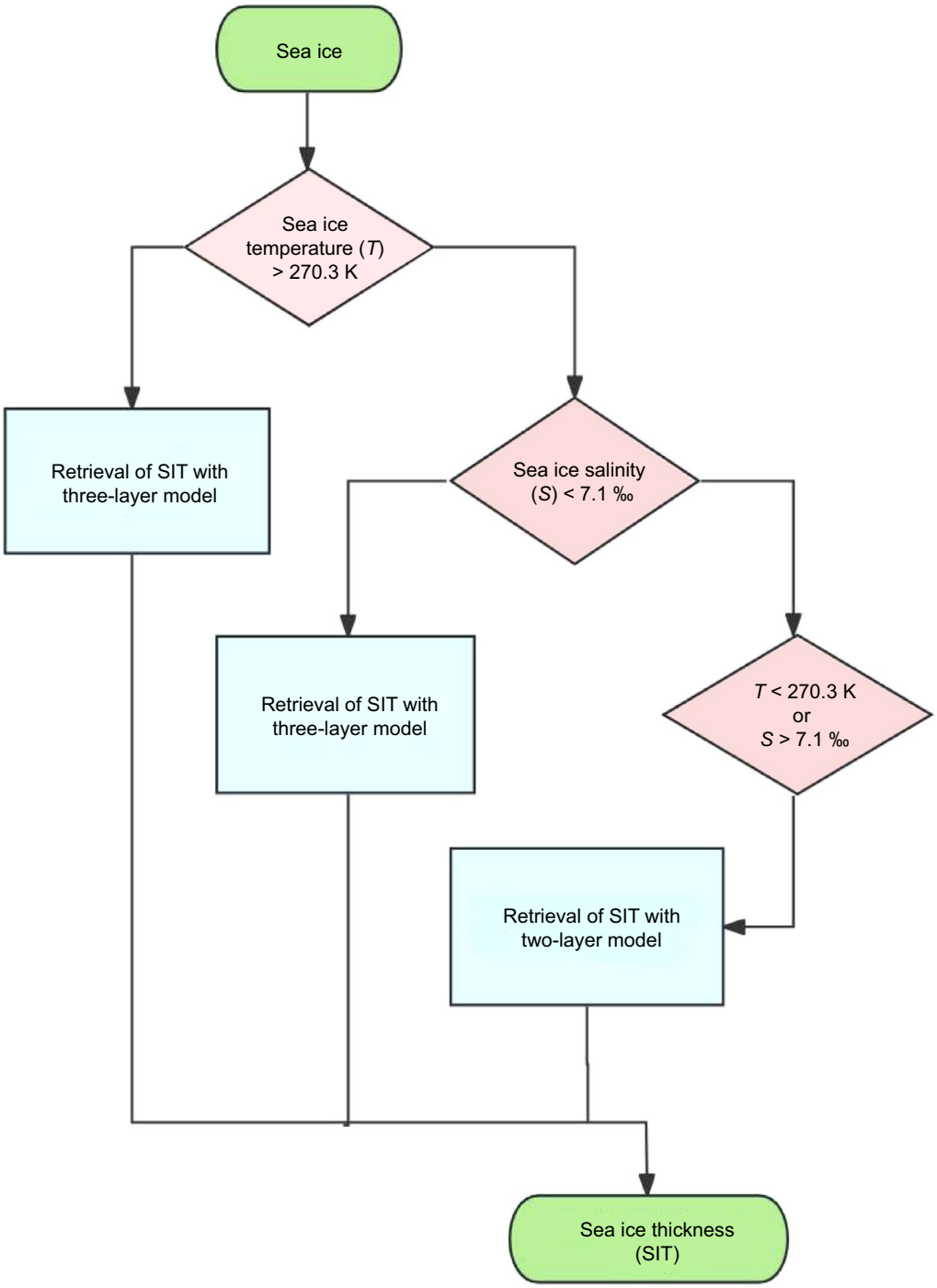

Fig. 8 Schemes of the combined model. Based on *S* and *T*, a three-layer model is used to retrieve SIT when *T* is greater than 270.3 K or *S* is less than 7.1 ‰, while a two-layer model is used to retrieve SIT when *T* is less than 270.3 K or *S* is greater than 7.1 ‰

et al. (2023), the reflectivity from GPS, BDS, and Galileo is essentially similar when the Sea Ice Concentration (SIC) exceeds 15%. However, even with comparable performance under certain conditions, subtle differences between these systems could introduce discrepancies. The factors like variations in signal frequency or power, satellite orbital dynamics, antenna patterns, among others, might contribute to these disparities. Furthermore, each system's unique operational constraints or anomalies could impact data quality and consistency. Therefore,

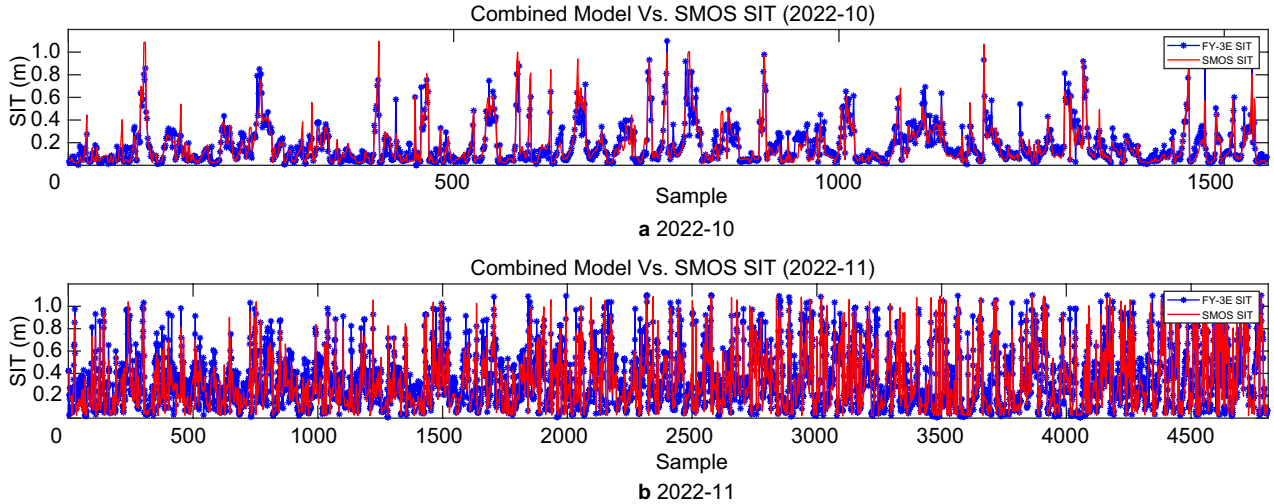

Fig. 9 Comparison of the combined model SIT and the reference SIT. Combined model retrieved SIT and SMOS SIT match well

ignoring these system-specific nuances when applying a uniform model for SIT retrieval may lead to errors, emphasizing the need for corrections or adjustments when combining GNSS-R data from multiple systems for more accurate and reliable SIT estimations.

Last, the most established models for SIT retrieval using GNSS-R data make certain assumptions about the environment. Two common assumptions are that the sea water surface is calm and the SIT distribution is uniform. These assumptions simplify the modelling process but do not always reflect real-world conditions. The sea surface state can vary significantly due to wind and wave conditions. Rough seas can cause additional scattering of GNSS signals, complicating their interpretation. Wind also affects sea ice dynamics, leading to non-uniformities in SIT. Similarly, SIT can be highly variable even within a small geographic area due to factors such as ice growth, melting processes, or dynamic interactions between ice floes. This variability further complicates the SIT retrieval from GNSS-R data. Addressing these complexities requires improving the existing models or developing of new ones that better account for these variables.

Conclusion

GNSS-R has been widely utilized for remote sensing applications over land and oceans. While there is considerable research on spaceborne GNSS-R for sea ice detection, including its identification, classification, distribution, and concentration, there exists a noticeable gap in addressing Sea Ice Thickness (SIT), a particularly challenging parameter to detect. Consequently, research on SIT inversion methods using spaceborne GNSS-R holds significant scientific and practical values.

This study aims to refine the two-layer model by developing a three-layer medium model of air-sea ice-seawater. The three-layer model incorporates the upper interracial reflections, which are neglected in the two-layer model, into the modeling process.

SIT estimation using FY-3E GNOS-R data employed both the two- and three-layer models. The two-layer model yielded an RMSE of 0.162 m and a correlation coefficient (r) of 0.789 compared to the reference SIT. In contrast, the three-layer model showed a better performance for thicker SIT, with an RMSE of 0.149 m and the r of 0.830. To exploit their respective strengths, a combined model was devised, resulting in a better accuracy (RMSE of 0.137 m and r of 0.852) for SIT estimation. This fusion scheme enhances the FY-3E GNOS-R's capability to retrieve SIT with better precision.

In the future, as GNSS-R technology advances, there is an expectation to develop a four-layer model encompassing air, snow, sea ice, and sea water. This enhanced model aims to retrieve SIT more accurately, providing a nuanced representation of polar sea-ice conditions while maintaining estimation accuracy. The poorer performance of the three-layer model is possibly attributed to negative freeboard, which can be addressed by refining the calculation of R_1. Future endeavors may tackle this issue through in situ measurements of SIT data or improved remote sensing products. Additionally, efforts can be made to independently retrieve SITs by GNSS-R without external data, focusing on obtaining sea ice temperature and salinity.

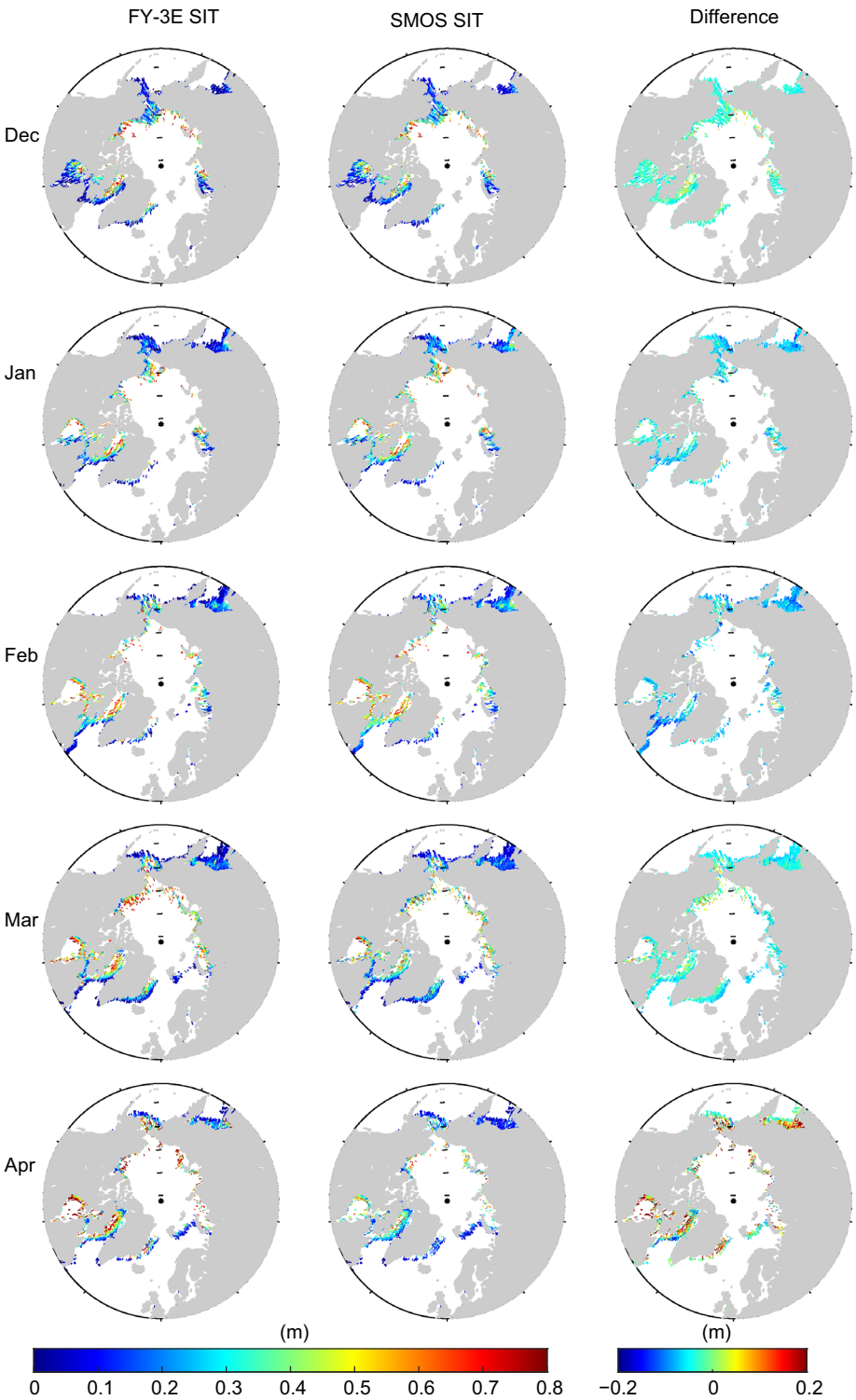

Fig. 10 Contrast between the SIT derived from the combined model and the reference SIT. In March and April, due to the effect of warmer temperatures, the SMOS SIT itself becomes more error-prone, so that the SIT retrieved in combination with the model shows some significant deviations from the SMOS SIT

Acknowledgements
The authors would like to acknowledge the National Satellite Meteorological Center for making their FY-3E GNOS-II data available.

Author contributions
YX conducted the experiments, performed validation, and drafted the paper. QY conceived the idea and provided assistance throughout the study. All authors read and approved the final manuscript.

Funding
This research was funded by the National Natural Science Foundation of China under Grant 42001362.

Availability of data and materials
The data that support the findings of this study are available from the National Satellite Meteorological Center (NSMC) which can be accessed at https://satellite.nsmc.org.cn.

Declarations

Competing interests
The authors declare that they have no competing interests.

Received: 14 September 2023 Accepted: 25 April 2024
Published online: 10 June 2024

References

Camps, A., Park, H., Pablos, M., Foti, G., Gommenginger, C. P., Liu, P. W., & Judge, J. (2016). Sensitivity of GNSS-R spaceborne observations to soil moisture and vegetation. *IEEE Journal of Selected Topics in Applied Earth Observations and Remote Sensing, 9*(10), 4730–4742.

Fung, A. K., Tjuatja, S., Beaven, S., Gogineni, S. P., Jezek, K., Gow, A. J., & Perovich, D. K. (1994, August). Modeling interpretation of scattering from snow-covered sea ice. In *Proceedings of IGARSS'94–1994 IEEE international geoscience and remote sensing symposium* (Vol. 1, pp. 617–619). IEEE.

Garrison, J. L., Komjathy, A., Zavorotny, V. U., & Katzberg, S. J. (2002). Wind speed measurement using forward scattered GPS signals. *IEEE Transactions on Geoscience and Remote Sensing, 40*(1), 50–65.

Hartmann, D.L., Tank, A.M.K., Rusticucci, M., Alexander, L.V., Brönnimann, S., Charabi, Y.A.R., Dentener, F.J., Dlugokencky, E.J., Easterling, D.R., Kaplan, A., Soden, B.J. & Zhai, P. (2013). Observations: atmosphere and surface. In *Climate change 2013 the physical science basis: Working group I contribution to the fifth assessment report of the intergovernmental panel on climate change* (pp. 159–254). Cambridge University Press.

Jin, S., & Najibi, N. (2014). Sensing snow height and surface temperature variations in Greenland from GPS reflected signals. *Advances in Space Research, 53*(11), 1623–1633.

Jin, S., Qian, X., & Kutoglu, H. (2016). Snow depth variations estimated from GPS-Reflectometry: A case study in Alaska from L2P SNR data. *Remote Sensing, 8*(1), 63.

Kaleschke, L., Tian-Kunze, X., Maaß, N., Beitsch, A., Wernecke, A., Miernecki, M., Müller, G., Fock, B. H., Gierisch, A. M., Schlünzen, K. H., Pohlmann, T., & Casal, T. (2016). SMOS sea ice product: Operational application and validation in the Barents Sea marginal ice zone. *Remote Sensing of Environment, 180*, 264–273.

Katzberg, S. J., Torres, O., Grant, M. S., & Masters, D. (2006). Utilizing calibrated GPS reflected signals to estimate soil reflectivity and dielectric constant: Results from SMEX02. *Remote Sensing of Environment, 100*(1), 17–28.

Klein, L., & Swift, C. (1977). An improved model for the dielectric constant of sea water at microwave frequencies. *IEEE Transactions on Antennas and Propagation, 25*(1), 104–111.

Larson, K. M., Gutmann, E. D., Zavorotny, V. U., Braun, J. J., Williams, M. W., & Nievinski, F. G. (2009). Can we measure snow depth with GPS receivers? *Geophysical Research Letters*, *36*(17).

Laxon, S., Peacock, N., & Smith, D. (2003). High interannual variability of sea ice thickness in the Arctic region. *Nature, 425*(6961), 947–950.

Li, C., & Huang, W. (2014). An algorithm for sea-surface wind field retrieval from GNSS-R delay-Doppler map. *IEEE Geoscience and Remote Sensing Letters, 11*(12), 2110–2114.

Li, S., Dou, T., & Xiao, C. (2021). A preliminary investigation of Arctic sea ice negative freeboard from in-situ observations and radar altimetry. *Journal of Ocean University of China, 20*, 307–314.

Li, Z., Guo, F., Chen, F., Zhang, Z., & Zhang, X. (2023). Wind speed retrieval using GNSS-R technique with geographic partitioning. *Satellite Navigation, 4*(1), 4.

Tian-Kunze, X., Kaleschke, L. (2021). SMOS Sea Ice Thickness ReadMe-First Technical Note (RM-TN). Retrieved 12 June, 2024, from https://www.cen.uni-hamburg.de/en/icdc/data/cryosphere/docs-cryo/awi-esa-smos-rm-tn-v2-0-final.pdf.

Tian-Kunze, X., Kaleschke, L., Maaß, N., Mäkynen, M., Serra, N., Drusch, M., & Krumpen, T. (2014). SMOS-derived thin sea ice thickness: Algorithm baseline, product specifications and initial verification. *The Cryosphere, 8*(3), 997–1018.

Tietsche, S., Alonso-Balmaseda, M., Rosnay, P., Zuo, H., Tian-Kunze, X., & Kaleschke, L. (2018). Thin Arctic sea ice in L-band observations and an ocean reanalysis. *The Cryosphere, 12*(6), 2051–2072.

Tilling, R. L., Ridout, A., & Shepherd, A. (2016). Near-real-time Arctic sea ice thickness and volume from CryoSat-2. *The Cryosphere, 10*(5), 2003–2012.

Tsang, L., & Newton, R. W. (1982). Microwave emissions from soils with rough surfaces. *Journal of Geophysical Research: Oceans, 87*(C11), 9017–9024.

Ulaby, F. T., Moore, R. K., & Fung, A. K. (1986). *Microwave remote sensing: Active and passive*. (Vol. 2). Addison-Wesley Pub. Co., Advanced Book Program/World Science Division.

Vant, M. R., Ramseier, R. O., & Makios, V. (1978). The complex-dielectric constant of sea ice at frequencies in the range 0.1–40 GHz. *Journal of Applied Physics, 49*(3), 1264–1280.

Xie, T., Perrie, W., Wei, C., & Zhao, L. (2020). Discrimination of open water from sea ice in the Labrador Sea using quad-polarized synthetic aperture radar. *Remote Sensing of Environment, 247*, 111948.

Xie, Y., & Yan, Q. (2024). Stand-alone retrieval of sea ice thickness from FY-3E GNOS-R data. *IEEE Geoscience and Remote Sensing Letters, 21*(5), 1–5.

Yan, Q., & Huang, W. (2019). Sea ice remote sensing using GNSS-R: A review. *Remote Sensing, 11*(21), 2565.

Yan, Q., & Huang, W. (2020). Sea ice thickness measurement using spaceborne GNSS-R: First results with TechDemoSat-1 data. *IEEE Journal of Selected Topics in Applied Earth Observations and Remote Sensing, 13*, 577–587.

Yan, Q., Huang, W., & Foti, G. (2017). Quantification of the relationship between sea surface roughness and the size of the glistening zone for GNSS-R. *IEEE Geoscience and Remote Sensing Letters, 15*(2), 237–241.

Yan, Q., Huang, W., Jin, S., & Jia, Y. (2020). Pan-tropical soil moisture mapping based on a three-layer model from CYGNSS GNSS-R data. *Remote Sensing of Environment, 247*, 111944.

Yin, C., Huang, F., Xia, J., Bai, W., Sun, Y., Yang, G., Zhai, X., Xu, N., Hu, X., Zhang, P., Wang, J., & Cai, Y. (2023). Soil moisture retrieval from multi-GNSS reflectometry on FY-3E GNOS-II by land cover classification. *Remote Sensing, 15*(4), 1097.

Zavorotny, V. U., Gleason, S., Cardellach, E., & Camps, A. (2014). Tutorial on remote sensing using GNSS bistatic radar of opportunity. *IEEE Geoscience and Remote Sensing Magazine, 2*(4), 8–45.

Publisher's Note